

Dielectric constant and ac conductivity of the layered cobalt oxide $\text{Bi}_2\text{Sr}_2\text{CoO}_{6+\delta}$: A possible metal-dielectric composite made by self-organization of Co^{2+} and Co^{3+} ions

Y. Nagao and I. Terasaki*

Department of Applied Physics, Waseda University, Tokyo 169-8555, Japan

T. Nakano

 Department of Applied Physics, Waseda University, Tokyo 169-8555, Japan
 and CREST, Japan Science and Technology Agency, Kawaguchi 332-0012, Japan

(Received 7 February 2007; revised manuscript received 9 July 2007; published 10 October 2007)

The dielectric constant and ac conductivity of a single-crystal sample of the layered cobalt oxide $\text{Bi}_2\text{Sr}_2\text{CoO}_{6+\delta}$ were measured along the c axis from 10^2 to 10^9 Hz from 110 to 300 K, the frequency dependence of which is found to be similar to that for metal-dielectric composites. The ac conductivity obeys the same scaling relation as that of disordered solids, which is quantitatively consistent with a theoretical calculation for spatially inhomogeneous conductive medium. This implies that the charge carrier on the Co^{2+} site is electronically segregated in the CoO_2 plane. This compound can work as a metal-dielectric composite even in a form of single crystal, a possible mechanism of which is suggested on the basis of the electronic configuration of Co ions.

DOI: 10.1103/PhysRevB.76.144203

PACS number(s): 72.80.Ga, 72.80.Ng, 77.84.Lf

I. INTRODUCTION

Cobalt oxides are interesting materials from the viewpoints of basic science and technological application, because different valences are tightly bound with different properties. The Co^{3+} ions have nearly degenerate spin states in LaCoO_3 [the low-spin state of $(e_g)^0(t_{2g})^6$ and the high-spin state of $(e_g)^2(t_{2g})^4$],¹ which often causes spin-state transition and/or crossover against temperature² and pressure.³ The Co^{4+} ions are mostly in the low-spin state, which are responsible for metallic conduction. Typical examples are itinerant ferromagnetic state in $\text{La}_{1-x}\text{Sr}_x\text{CoO}_3$,⁴ large thermopower in Na_xCoO_2 ,⁵ and superconductivity in $\text{Na}_x\text{CoO}_2 \cdot y\text{H}_2\text{O}$.⁶ In contrast, the Co^{2+} ions are stable as the high-spin state, which drive the system to be a magnetic insulator. For the intermediate valence between Co^{2+} and Co^{3+} , carriers are often confined on the Co^{2+} sites, as is observed in the charge and/or spin order in $\text{La}_{1.5}\text{Sr}_{0.5}\text{CoO}_4$,⁷ small polarons in $\text{Ca}_2(\text{Co},\text{Al})_2\text{O}_5$,⁸ and charge segregation in $\text{Sr}_2\text{Cu}_2\text{CoO}_2\text{S}_2$.⁹

The layered cobalt oxide $\text{Bi}_2\text{Sr}_2\text{CoO}_{6+\delta}$ is one of such interesting materials.¹⁰ As is schematically shown in the inset of Fig. 1, the crystal structure is isomorphic to the superconducting copper oxide $\text{Bi}_2\text{Sr}_2\text{CoO}_{6+\delta}$. The Co ion is surrounded with the six oxygen ions, and the edge-shared CoO_6 octahedra form a square lattice of the CoO_2 plane along the a and b axes. The NaCl-type block layer of $\text{Bi}_2\text{Sr}_2\text{O}_4$ is alternately stacked with the CoO_2 plane along the c axis to make the layered structure. The formal cobalt valence of this oxide is between 2+ and 3+ and exhibits complicated magnetic and/or charge-ordered states at low temperatures.¹¹

Here, we report on the transport properties of well-characterized single crystals of $\text{Bi}_2\text{Sr}_2\text{CoO}_{6+\delta}$ mainly focusing on its ac response along the c axis. Previously, we found that the c -axis dielectric constant was fairly large (~ 60) at low frequencies, whose frequency dependence was similar to that of metal-dielectric composites.¹² We have ascribed this to the localized carriers on the Co^{2+} ions segregated in the

CoO_2 plane, which is quantitatively consistent with a small-polaron picture suggested from the observed resistivity and thermopower.

II. EXPERIMENT

Single crystals of $\text{Bi}_2\text{Sr}_2\text{CoO}_{6+\delta}$ were grown by a floating zone method. A polycrystalline stoichiometric feed rod was prepared by a solid-state reaction. A stoichiometric mixture of Bi_2O_3 , SrCO_3 , and Co_3O_4 powders was calcined at 850 °C for 12 h in air and was crushed and ground carefully after cooling down to room temperature. It was calcined

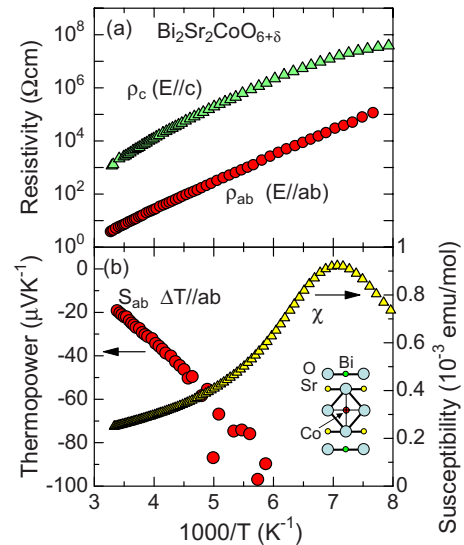


FIG. 1. (Color online) (a) In-plane resistivity (ρ_{ab}) and out-of-plane resistivity (ρ_c) and (b) in-plane thermopower (S_{ab}) and susceptibility (χ) of single-crystal samples of $\text{Bi}_2\text{Sr}_2\text{CoO}_{6+\delta}$. The crystal structure is schematically shown in the inset.

again at 890 °C for 12 h in air and was finally sintered into the feed rod at 900 °C for 48 h in air. The crystal was grown with a velocity of 0.5 mm/h in a mixed gas flow of O₂(20%) and Ar(80%), the composition of which was determined to be Bi:Sr:Co=2.1:2.0:1.0 by energy dispersive x-ray analysis. Single crystals with a typical size of 1 × 1 × 0.05 mm³ were used for transport experiments.

The resistivity ρ was measured with a four-probe method in a constant voltage of 1 V from 110 to 300 K, and the thermopower S was measured using a steady-state method with a typical temperature gradient of 1 K/mm from 170 to 300 K in a liquid-He cryostat. The susceptibility was measured in an external magnetic field of 0.1 T with a commercial superconducting quantum interference device susceptometer (Quantum Design magnetic property measurement system). The complex impedance was measured with a two-probe technique in a frequency range of 10²–10⁹ Hz from 110 to 300 K in a closed-cycle refrigerator. A conventional *LCR* meter (Agilent 4284A) was used below 1 MHz and a radio-frequency *LCR* meter (Agilent 4287A) above 1 MHz. We used a similar technique as Böhmer *et al.*¹³ reported and successfully subtracted the contribution of the impedance of the measurement circuit by measuring three standard samples [open (0S), short (0 Ω), and load (50 Ω)] in advance.¹⁴ A low contact resistance was realized by uniformly painting the silver paste (Dupont 6838) on both sides of the *ab*-plane surface, followed by annealing at 873 K for 30 min. We attached four probes on the sample to measure the four-probe and two-probe resistances in advance, from which the contact resistance was evaluated to be 5–10 Ω . This can be safely neglected in comparison with the sample resistance (typically more than 500 Ω). Note that we measured the complex impedance only along the *c* axis. A necessary condition to measure the real and imaginary parts of the impedance is that the resistance and reactance components of the sample are of the same order, which is reduced to the condition of $\omega\rho\varepsilon \sim 1$, where ω and ε are the angular frequency and the dielectric constant. To satisfy this condition, ρ should be as high as 10⁴ Ω cm for $\varepsilon/\varepsilon_0=10^2$ at $f=\omega/2\pi=10^6$ Hz, which means that the in-plane resistivity is too small to measure ε precisely, unless ε is huge. For a conductive sample, ε is often observed to be huge, which is an artifact due to the charge depletion near the electrical contact.¹⁵

III. RESULTS AND DISCUSSION

Figure 1(a) shows the Arrhenius plot of the *ab*-plane resistivity (ρ_{ab}) and the *c*-axis resistivity (ρ_c), clearly indicating that ρ_{ab} and ρ_c are well characterized by an activation-type transport near room temperature. Reflecting the two-dimensional electronic states, ρ_c is about 300 times larger than ρ_{ab} at room temperature, while the slope is nearly the same, as is usually seen in various layered semiconducting oxides.^{8,16,17} Figure 1(b) shows the in-plane thermopower (S_{ab}) plotted as a function of $1/T$. The negative sign suggests that the majority carrier of this material is an electron, being consistent with other Co²⁺-Co³⁺-based oxides.⁸ S_{ab} is

roughly linear in $1/T$, also indicating an activation-type transport. The activation energy is, however, different from that evaluated from ρ , which can be obtained from the relations given by

$$\rho = \rho_0 \exp\left(\frac{E_g^R}{k_B T}\right), \quad (1)$$

$$S = S_0 + \frac{E_g^S}{eT}, \quad (2)$$

where E_g^R and E_g^S are the activation energies for ρ and S . The term S_0 represents the entropy per site given by the Heikes formula. From the slopes in Fig. 1, E_g^R is evaluated to be 0.19 eV along the *ab* direction and 0.21 eV along the *c* axis, whereas E_g^S is evaluated to be a much smaller value of 0.028 eV. The relation of $E_g^S \ll E_g^R$ implies that the electric conduction is dominated by small polarons with a polaron binding energy of $E_g^R - E_g^S \sim 0.16$ eV,¹⁸ which is comparable with the binding energy for other Co²⁺-Co³⁺-based oxides such as Ca₂(Co,Al)₂O₅.⁸

The small value of E_g^S roughly reflects a small energy gap in the density of states, which is comparable to the thermal energy at room temperature. This implies that the charge transport would be essentially metallic near room temperature, in the sense that there is no energy gap at the chemical potential. In this context, we can expect this compound to have conduction carriers although they are confined near the Co²⁺ sites by the polaron binding energy. According to the neutron diffraction,¹¹ the Co³⁺ ions are inhomogeneously distributed in the CoO₂ plane, while the Co²⁺ ions form a spin stripe. Thus, we may regard the Co²⁺-rich domain as a “metallic” domain and the Co³⁺-rich domain as a dielectric (or insulating) domain.

The susceptibility of a sample from the same batch is shown in Fig. 1(b), which shows an antiferromagnetic transition near 150 K ($=T_N$). This temperature is almost the same as that of samples prepared in air by Tarascon *et al.*¹⁰ and that of an as-grown crystal by Shi *et al.*¹⁹ The physical properties of Bi₂Sr₂CoO_{6+ δ} are sensitive to oxygen nonstoichiometry δ , which is roughly determined by the Néel temperature.¹¹ By comparing T_N with the previous works, we evaluate δ of our sample to be 0.35 ± 0.05 , which indicates that the ratio of Co³⁺:Co²⁺ is in the range from 6:4 to 8:2. We should note that the evaluated δ is consistent with the phase diagram studied by Zinkevich *et al.*²⁰

Figure 2 shows the dielectric constant ε and the ac conductivity σ along the *c* axis as a function of frequency f at various temperatures. The data are smoothly connected at 1 MHz within reasonable accuracy (error less than 10%), though the two *LCR* meters were used for the different frequency ranges. The magnitude is fairly large at low frequencies, which is comparable with the *c*-axis dielectric function of the insulating copper oxide Bi₂Sr₂DyCu₂O₈.¹⁴ We did not obtain a very large value of 10³–10⁴ reported by Chern *et al.*²¹ Anomalously large dielectric constants are often “apparent,”¹⁵ and the contact and/or the depletion layer

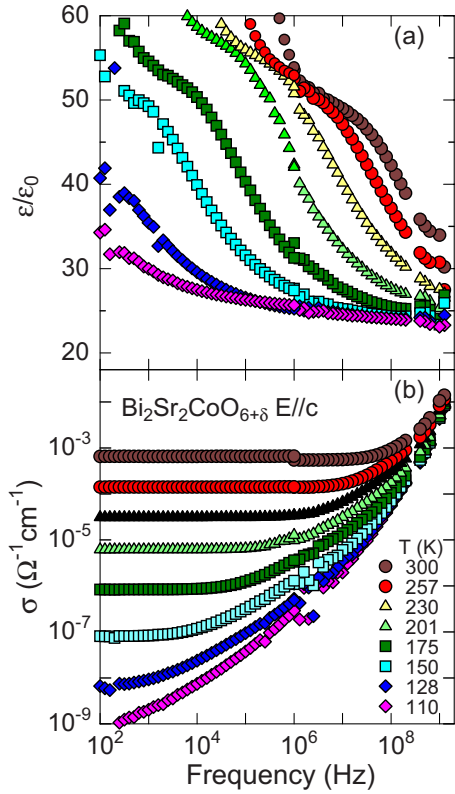


FIG. 2. (Color online) (a) Out-of-plane dielectric constant (ϵ) and (b) out-of-plane ac conductivity (σ) of a single-crystal sample of $\text{Bi}_2\text{Sr}_2\text{CoO}_{6+\delta}$.

might affect their measurement. In our measurement, the 100 Hz conductivity is quantitatively consistent with the dc conductivity measured by the four-probe method ($=1/\rho_c$) in Fig. 1(a), which further evidences that the contact resistance R_c was negligibly small.

The dielectric constant shows unusual frequency dependence in Fig. 2(a), where it decreases with increasing frequency with a cusp at a certain frequency and seems to saturate to a value of 25 in the high-frequency limit. The ac conductivity also shows unusual frequency dependence in Fig. 2(b), where it does not obey a power law of single exponent, but shows superlinear behavior at high frequencies. To our knowledge, the dielectric response of strongly correlated oxides has been explained in terms of dielectric relaxation²² or in terms of variable range hopping.²³ We should emphasize here that neither of the two can explain the data. Since $\sigma(\omega)$ cannot be described by a single exponent, $\sigma(\omega)$ is unlikely to come from a variable-range-hopping mechanism in which $\sigma(\omega) \propto \omega^s$ ($s < 1$) is expected.²³ We also note that $\text{Im } \epsilon \propto \sigma/\omega$ increases at high frequencies because of the superlinear behavior, which is difficult to explain by a single relaxation term.

We have found that the features in Fig. 2 are very similar to what is observed in metal-dielectric composites consisting of metallic and insulating nanoparticles, in which the real part of the capacitance exhibits similar relaxation and the imaginary part ($\propto \sigma/\omega$) shows a kink.²⁴ The ac conductivity $\sigma(\omega)$ of various disordered solids²⁵ including

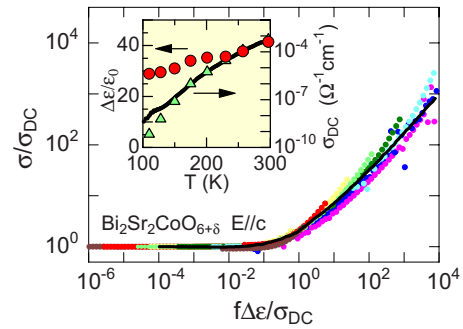


FIG. 3. (Color online) The Taylor-Isard scaling for the measured data shown in Fig. 2. The solid curve is a calculation for a random network of resistor and capacitor by Dyre (Ref. 28) $\Delta\epsilon$ and σ_{dc} are shown in the inset. The dc conductivity ($=1/\rho_c$) in Fig. 1 is also shown by the solid curve in the inset.

metal-dielectric composites obeys a scaling relation given by²⁶

$$\tilde{\sigma} \equiv \frac{\sigma(\omega)}{\sigma_{\text{dc}}} = F\left(\frac{C\omega}{\sigma_{\text{dc}}}\right), \quad (3)$$

where σ_{dc} and C are the dc conductivity and a scaling constant. Equation (3) is called the Taylor-Isard scaling and indicates that the ratio of the ac conductivity to the dc conductivity is written by a single scaling function $F(\tilde{\omega})$ against a properly normalized frequency $\tilde{\omega}$. Empirically, C is roughly proportional to the difference of the dielectric constants between low- and high-frequency limits $\Delta\epsilon = \epsilon_{\text{LF}} - \epsilon_{\text{HF}}$, and Sidebottom proposed the following scaling:²⁷

$$\frac{\sigma(\omega)}{\sigma_{\text{dc}}} = F\left(\frac{f\Delta\epsilon}{\sigma_{\text{dc}}}\right). \quad (4)$$

Figure 3 shows the scaling relation given by Eq. (4) for the same data in Fig. 2. We used the ac conductivity at 100 Hz for σ_{dc} , and thus took $\Delta\epsilon$ as only one fitting parameter. Clearly, all the curves fall onto a single scaling curve, indicating that the scaling explains the measured data excellently. The fitting parameters are plotted as a function of temperature in the inset of Fig. 3, which are converged to reasonable values: Weakly temperature-dependent $\Delta\epsilon$ quantitatively corresponds to the difference of the dielectric constant between low and high frequencies. σ_{dc} excellently coincides with the c -axis dc conductivity ($=1/\rho_c$) measured in Fig. 1, as shown by the solid curve in the inset. Accordingly, we conclude that the Taylor-Isard scaling satisfactorily explains the temperature and frequency dependence of the complex c -axis conductivity of $\text{Bi}_2\text{Sr}_2\text{CoO}_{6+\delta}$, or equivalently, this material can work as a metal-dielectric composite even in a form of single crystal. We further note that this scaling does not always work well for other transition-metal oxides: For example, Debye-type relaxation is seen in ϵ of the charge-ordered Mn oxide $(\text{Pr}, \text{Ca})\text{MnO}_3$,²² which suggests that polaronic conduction is not a necessary condition for good fit to the Taylor-Isard scaling.

Let us compare the scaling function obtained here with a theoretical calculation. Dyre²⁸ calculated a spatially randomly varying conductivity in metal-dielectric composite within the effective medium approximation and found the scaling function $\tilde{\sigma}$,

$$\tilde{\sigma} \ln \tilde{\sigma} = \tilde{\omega}, \quad (5)$$

as a function of properly normalized frequency $\tilde{\omega}$, as shown by the solid curve in Fig. 3. The theoretical calculation is in excellent agreement with the data, which strongly suggests that the conductivity is spatially inhomogeneous in the title compound, and the electric response can be understood in terms of a random network of resistor and capacitor that mimics electrical features of metal-dielectric composites.

Finally, we wish to propose a possible origin for the dielectric response in $\text{Bi}_2\text{Sr}_2\text{CoO}_{6+\delta}$. As mentioned previously, this material includes Co^{3+} and Co^{2+} ions, and the Co^{2+} -rich and Co^{3+} -rich domains can be regarded as a metallic and a dielectric domain, respectively. The Co^{3+} ion is magnetic (high-spin state or intermediate-spin state) and the Co^{2+} ion is in the high-spin state of $(e_g)^2(t_{2g})^5$. If the Co^{3+} ion is in the high-spin state of $(e_g)^2(t_{2g})^4$, the highly localized t_{2g} electron finds it difficult to hop between the Co^{2+} and Co^{3+} ions. If the Co^{3+} ion is in the intermediate-spin state of $(e_g)^1(t_{2g})^5$, one e_g electron may hop via double exchange mechanism from Co^{2+} to Co^{3+} . In this case, however, the intermediate-spin-state Co^{3+} ion is strongly coupled with Jahn-Teller distortion, so that the carriers act as a Jahn-Teller polaron. In either case, Co^{2+} - Co^{3+} -based materials often become a small-polaron conductor, in which the d electrons are confined at the Co^{2+} site. Similar confinement was already discussed in $\text{HoBaCo}_2\text{O}_{5.5}$ by Maignan *et al.*,²⁹ which may

cause different dielectric response from the Mn oxide.²² As a result, the charge distribution becomes spatially inhomogeneous, as was revealed from the neutron experiment.¹¹

IV. SUMMARY

In summary, we prepared single crystals of the layered cobalt oxide $\text{Bi}_2\text{Sr}_2\text{CoO}_6$ by a floating-zone method and measured resistivity, thermopower, dielectric constant, and ac conductivity. The dc transport is explained by a polaron conduction with a polaron binding energy of 0.16 eV, which is consistent with other Co^{2+} - Co^{3+} -based oxides. The dielectric constant and ac conductivity are very similar to those of metal-dielectric composite, which obeys the same scaling relation as that for disordered solids in which the conductivity is spatially inhomogeneous. This implies that the charge distribution is highly inhomogeneous in the sample, which is consistent with the highly localized nature of polarons on the Co^{2+} sites. We have explained the ac response in terms of metal-dielectric composite and consistently explain, at least qualitatively, the dc transport parameters and the magnetic order studied by Thomas *et al.*¹¹ Since our model is based on macroscopic measurements, it is waiting for some microscopic measurements such as scanning tunneling microscopy or NMR.

ACKNOWLEDGMENTS

The authors would like to thank W. Kobayashi, S. Okada, and S. Koga for fruitful discussion on the universality of ac conduction and D. Khomskii for fruitful discussion on the electronic state of Co^{2+} . This work was partially supported by MEXT, the Grant-in-Aid for Scientific Research (No. 17340114 and No. 16076213).

*terra@waseda.jp

¹J. B. Goodenough, *J. Phys. Chem. Solids* **6**, 287 (1958).

²K. Asai, A. Yoneda, O. Yokokura, J. M. Tranquada, G. Shirane, and K. Kohn, *J. Phys. Soc. Jpn.* **67**, 290 (1998).

³T. Vogt, J. A. Hriljac, N. C. Hyatt, and P. Woodward, *Phys. Rev. B* **67**, 140401(R) (2003).

⁴M. Kriener, C. Zobel, A. Reichl, J. Baier, M. Cwik, K. Berggold, H. Kierspel, O. Zabara, A. Freimuth, and T. Lorenz, *Phys. Rev. B* **69**, 094417 (2004).

⁵I. Terasaki, Y. Sasago, and K. Uchinokura, *Phys. Rev. B* **56**, R12685 (1997).

⁶K. Takada, H. Sakurai, E. Takayama-Muromachi, F. Izumi, R. A. Dilanian, and T. Sasaki, *Nature (London)* **422**, 53 (2003).

⁷I. A. Zaloznyak, J. P. Hill, J. M. Tranquada, R. Erwin, and Y. Moritomo, *Phys. Rev. Lett.* **85**, 4353 (2000).

⁸W. Kobayashi, A. Satake, and I. Terasaki, *Jpn. J. Appl. Phys., Part 1* **41**, 3025 (2002).

⁹S. Okada, I. Terasaki, H. Okabe, and M. Matoba, *J. Phys. Soc. Jpn.* **74**, 1525 (2005).

¹⁰J. M. Tarascon *et al.*, *Phys. Rev. B* **39**, 11587 (1989).

¹¹K. J. Thomas, Y. S. Lee, F. C. Chou, B. Khaykovich, P. A. Lee, M. A. Kastner, R. J. Cava, and J. W. Lynn, *Phys. Rev. B* **66**,

054415 (2002).

¹²I. Terasaki, *Physica B* **383**, 107 (2006).

¹³R. Böhmer, M. Maglione, P. Lunkenheimer, and A. Loidl, *J. Appl. Phys.* **65**, 901 (1989).

¹⁴T. Takayanagi, M. Kogure, and I. Terasaki, *J. Phys.: Condens. Matter* **14**, 1361 (2002).

¹⁵P. Lunkenheimer, V. Bobnar, A. V. Pronin, A. I. Ritus, A. A. Volkov, and A. Loidl, *Phys. Rev. B* **66**, 052105 (2002).

¹⁶C. N. R. Rao, D. J. Buttrey, N. Otsuka, P. Ganguly, H. R. Harrison, C. J. Sandberg, and J. M. Honig, *J. Solid State Chem.* **51**, 266 (1984).

¹⁷Y. Watanabe, D. C. Tsui, J. T. Birmingham, N. P. Ong, and J. M. Tarascon, *Phys. Rev. B* **43**, 3026 (1991).

¹⁸T. T. M. Palstra, A. P. Ramirez, S.-W. Cheong, B. R. Zegarski, P. Schiffer, and J. Zaanen, *Phys. Rev. B* **56**, 5104 (1997).

¹⁹J. B. Shi, J. C. Ho, T. J. Lee, B. S. Chiou, and H. C. Ku, *Physica C* **205**, 129 (1993).

²⁰M. V. Zinkevich, S. A. Prodan, Yu. G. Zonov, and V. V. Vashook, *J. Solid State Chem.* **136**, 1 (1998).

²¹G. Chern, L. R. Song, and J. B. Shi, *Physica C* **253**, 97 (1995).

²²S. Yamada, T. Arima, and K. Takita, *J. Phys. Soc. Jpn.* **68**, 3701 (1999).

- ²³C. Y. Chen, N. W. Preyer, P. J. Picone, M. A. Kastner, H. P. Jenssen, D. R. Gabbe, A. Cassanho, and R. J. Birgeneau, *Phys. Rev. Lett.* **63**, 2307 (1989).
- ²⁴A. B. Pakhomov, S. K. Wong, X. Yan, and X. X. Zhang, *Phys. Rev. B* **58**, R13375 (1998).
- ²⁵P. Lunkenheimer and A. Loidl, *Phys. Rev. Lett.* **91**, 207601 (2003).
- ²⁶J. C. Dyre and T. B. Schröder, *Rev. Mod. Phys.* **72**, 873 (2000), and references therein.
- ²⁷D. L. Sidebottom, *Phys. Rev. Lett.* **82**, 3653 (1999).
- ²⁸J. C. Dyre, *Phys. Rev. B* **48**, 12511 (1993).
- ²⁹A. Maignan, V. Caignaert, B. Raveau, D. Khomskii, and G. Sawatzky, *Phys. Rev. Lett.* **93**, 026401 (2004).